Marine Geology 271 (2010) 44–54

Contents lists available at ScienceDirect

Marine Geology

journal homepage: www.elsevier.com/locate/margeo

Reconstruction of retreating mass wasting in response to progressive slope steepening of the northeastern Cretan margin, eastern Mediterranean

Frank Strozyk [a,*], Michael Strasser [a], Sebastian Krastel [b], Mathias Meyer [b], Katrin Huhn [a]

[a] MARUM, Centre for Marine Environmental Sciences, Cluster of Excellence: The Ocean in the Earth System, University of Bremen, P.O. Box 33 04 40, D-28359 Bremen, Germany
[b] IFM-GEOMAR, Leibniz Institute of Marine Sciences, Cluster of Excellence: The Future Ocean, Christian-Albrecht-University Kiel, D-24148 Kiel, Germany

ARTICLE INFO

Article history:
Received 3 July 2009
Received in revised form 25 January 2010
Accepted 29 January 2010
Available online 6 February 2010

Communicated by D.J.W. Piper

Keywords:
Cretan Sea
landslides
slope architecture
slope failure
mass wasting

ABSTRACT

In this study we aim on a reconstruction of mechanisms and kinematics of slope-failure and mass-movement processes along the northeastern slope of Crete in the Hellenic forearc, eastern Mediterranean. Here, subsidence of the forearc basin and the uplift of the island of Crete cause ongoing steepening of the slope in-between. The high level of neotectonic activity in this region is expected to exert a key role in slope-failure development. Newly acquired reflection seismic data from the upper slope region reveal an intact sediment cover while the lower slope is devoid of both intact strata and mass-transport deposits (MTDs). In a mid-slope position, however, we found evidence for a ~4-km³-sized landslide complex that comprises several MTDs from translational transport of coherent sediment bodies over short distances. Morphometric analysis of these MTDs and their source scars indicates that this part of the northeast Cretan slope can be characterized as a cohesive slope. Furthermore, we reconstruct retrogressive development for this complex and determine a critical slope angle for both pre-conditioning of failure and subsequent landslide deposition near source scars. Consequently, data imply that the investigated shallower slope is stable due to low angles in the order of 3°, whereas 5°-inclined mid-slope portions favour both slope destabilization and landslide deposition. The failed mid-slope parts are dominated by sediment truncations from faults almost correlating with the orientation of head- and sidewalls of scars. We suggest that cohesive landslides and MTDs are generated and preserved, respectively, in such critical slope regions. If once generated, cohesive landslides reach the lower slope further downslope that exceeds the threshold gradient for MTD deposition (~5°), they are transported all the way down to the foot of the slope and disintegrate to mass flows. From these observations we suggest that the mass-wasting history of the investigated Cretan slope area over a longer period of time is characterized by repeated sediment erosion and transport into the deeper Cretan Sea basin. The relocation of the critical slope portion in upslope direction and therefore recurrence of mass-wasting events is thereby likely controlled by the progressive steepening of the slope. This mechanism and restriction of sediment failure to narrow, critically-inclined and relocating slope portions likely explains how such an active margin setting can exhibit only scarce findings of MTDs on the slope despite an expected, extensive and widespread mass wasting.

1. Introduction

It is generally accepted that repeated mass movements can erode a significant amount of submarine slope sediment through time and thus strongly affect slope morphology (e.g., Leeder, 1999; Canals et al., 2004; Haflidason et al., 2004; Urgeles et al., 2006). The mechanical behaviour of sediments and slope geometry thereby exert key roles in failure development and also have a high impact on the mass-movement transport mechanisms, which can occur either in a cohesive or disintegrative fashion (e.g., Locat and Lee, 2002; McAdoo et al., 2000). McAdoo et al. (2000, 2004) have shown that mass movements along active margin slopes bearing cohesive sediments often consist of compact landslides or slumps of low recurrence as these slopes can be of high resistance against shearing. Such cohesive landslides are of relatively small volumes and can have short runouts (e.g., Hampton et al., 1996 and Lee et al., 2007). Disintegration of landslides during longer runout as well as failure in sediments of non- or less-cohesive character can result in mass flows (e.g., Gee et al., 1999; Masson et al., 2006; Lee et al., 2007). Morphometric analyses of mass-transport deposits (MTDs), source scars and the adjacent slopes of cohesive landslides compared to mass flows indicate that they can strongly differ in scar geometry, headwall height and gradient, the gradient of the adjacent slope, as well as the mass-movement size and runout distance (McAdoo et al., 2000; Haflidason et al., 2003). Therefore, morphometric measurements on scars and MTDs can be used to reconstruct failure and transport kinematics as well as the

* Corresponding author. Now at the Geological Institut RWTH Aachen University, Wuellnerstr. 2, D-52056 Aachen, Germany. Tel.: +49 0241 80 95965.

0025-3227/$ – see front matter © 2010 Elsevier B.V. All rights reserved.
doi:10.1016/j.margeo.2010.01.008

mechanical behaviour of sediment during failure and transport (McAdoo et al., 2000).

The northeastern margin of Crete represents the southern border of the Cretan Sea submarine basin (Fig. 1A) and is an example that evidences only some scattered landslide scars and MTDs on an active margin slope. The detected pattern of MTDs on the slope comprises slides as well as debrites with volumes in the order of ≤0.5 to ≥2.0 km³ (e.g., Chronis et al., 2000; Kopf et al., 2006, 2007; Strozyk et al., 2009). Seismic data presented by Kopf et al. (2006) suggest the presence of stacked MTDs also in the deeper Cretan Sea sub-basins (i.e. the Kamilonisi and Heraklion Basin). However, the scarce findings of MTDs along the slope contrast the expectation of a diffuse and extensive mass-movement pattern related to the region's high neotectonic activity (e.g. earthquakes and tectonic movement), as characteristic for active margin settings. The high shear resistance of the cohesive, consolidated Cretan slope sediment is proposed being the responsible mechanism restricting a higher frequency of slope collapse (Chronis et al., 2000; Kopf et al., 2006, 2007).

The aim of this study is (i) an identification and detailed description of a cluster of MTDs on the northeastern Cretan slope, (ii) to measure proportions of MTDs, their source scars and the adjacent intact slope supported by morphometric analyses of this features, (iii) a determination of mass-movement types, runout distances and transport mechanisms, and (iv) to evaluate critical slope angles for sediment stability and pre-conditioning for its destabilization. Our study is based on the interpretation of multi-channel reflection seismic profiles and bathymetric data recorded during the 2006 CRESTS (Cretan Sea Tectonics and Sedimentology) cruise aboard R/V Poseidon. We also compare our findings to the concept of morphometric analysis of slope failures, and discuss the results in terms of slope morphology and tectonic movement representing pre-conditioning factors for mass wasting in such active margin environments.

2. Regional setting

The Cretan Sea basin represents the large forearc basin of the Hellenic subduction zone (McKenzie, 1978; Le Pichon and Angelier, 1979; Fig. 1A). This elongated, east–west-trending, almost north–south-extensional forearc depression is bordered to the north by the volcanic arc and to the south by the island of Crete (Fig. 1A and B), which is an exhumed horst structure (Bonneau, 1984) and still being uplifted (i.e. ≥6 mm a^{-1}; e.g., Ganas and Parsons, 2009 and references therein). Extension and subsidence of the basin is reconstructed to a last main creation phase during the Late Miocene and Pliocene, while it is proposed to have decreased since that time (Meulenkamp et al., 1988; Mascle and Martin, 1990). However, several surveys indicated recent fault activity and micro-seismicity in the southern Cretan Sea and have confirmed that the tectonic system is still active today (e.g. Lykousis et al., 1995; Perissoratis and Papadopoulos, 1999). Subsidence rates in the forearc region increase from the west to the east, likely associated to an increase of the dip of the African slab subduction to the east (e.g. Angelier et al., 1982; Meier et al., 2004). The resulting tectonic deformation to a southwest–northeast-striking half graben system (Fig. 1B) as well as Cretan Sea basin subsidence caused the formation of several large sub-basins, of which the Kamilonisi Basin is one of the deepest with up to 2500 m water depth (Fig. 1B; e.g. Stavrakakis et al., 2000). Major faults associated with these sub-basins as well as the Cretan Sea basin extension trend approximately northeast–southwest (Angelier et al., 1982; Mascle and Martin, 1990). A second system of faults trends

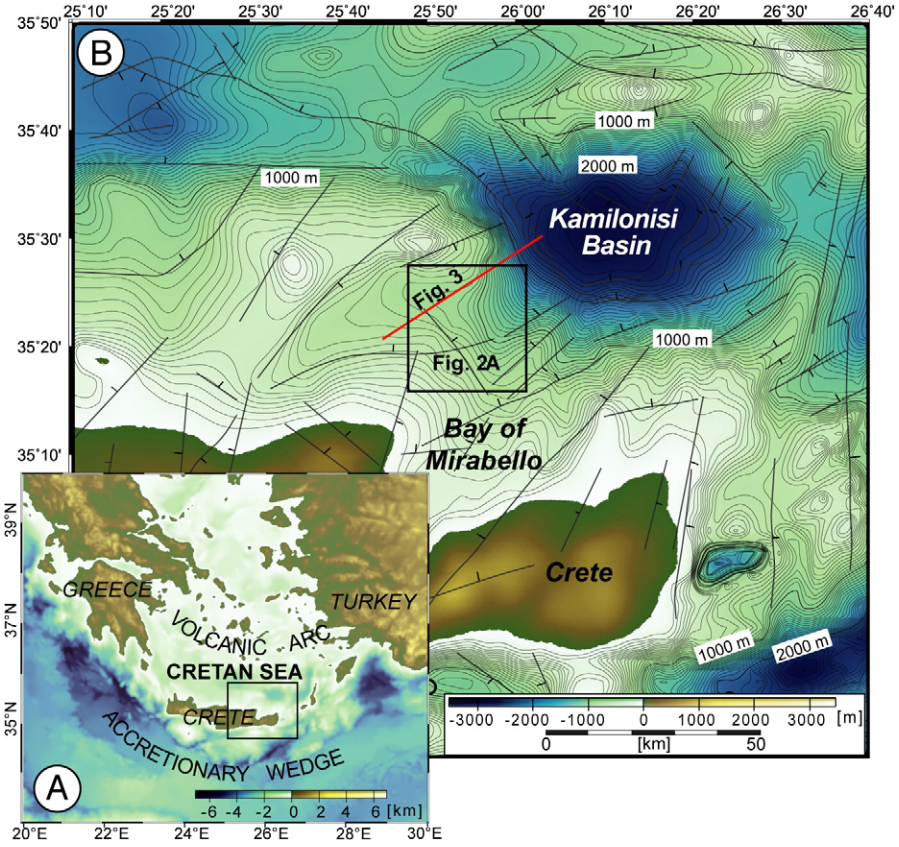

Fig. 1. A: Bathymetry map of the eastern Mediterranean active margin. The black box indicates the location of the study site and surroundings in the southern Cretan Sea (B); B: bathymetry map of the study site and surroundings on the northeastern margin of Crete, north of the Bay of Mirabello and southwest of the Kamilonisi Basin. Thin lines represent relief counter lines in 50-m intervals. Thick black lines indicate major faults in the southern Cretan Sea interpreted and compiled after Mascle and Martin (1990) and Angelier et al. (1982). The red line indicate the location of seismic profile GeoB06-133, the black box the outlines the study site in the mid-slope region (Fig. 2).

almost perpendicular southeast–northwest (Fig. 1B; Mascle and Martin, 1990). Owing to the extension in the forearc, the Cretan Sea sub-basin subsidence and the countering uplift of the island of Crete, the northern Cretan slope in-between is of steep and irregular topography (e.g., Chronis et al., 2000; Kopf et al., 2006; Strozyk et al., 2009).

3. Data and methods

3.1. Multibeam bathymetric data

Bathymetric mapping of the northeastern Cretan margin slope and the adjacent deeper Cretan basin was carried out during the CRESTS cruise with an ELAC SeaBeam 1050 multibeam echo-sounder (combined to conventional vessel GPS). This system was operated at 12 kHz with an auto-adjusting, maximum angular coverage of 150° corresponding to a swath width of up to 7.5 times the water depth. Bathymetric data of the investigated area (25°47′E–26°03′E/35°22′N–35°36′N) occupies about 700 m² of the northeastern Cretan slope in water depths between 200 and 1200 m. The data were processed with MB-System (Caress and Chayes, 1996) and gridded with resolutions of 10 and 20 m cell-sizes using GMT (Generic Mapping Tool; Wessel and Smith, 1998). Shaded relief plots of the bathymetric grid were used to identify, describe, and measure topographic and morphological seafloor features.

3.2. Seismic data

Reflection seismic profiles were recorded using a Mini-GI-Gun (2×0.25 l, 100–500 Hz, operated at 140–150 bars) and a 100 m-long 16-channel streamer with 8 hydrophones per channel and a group distance of 6.25 m. The shooting rate was 8 s, ship speed was about 4 kn and the resulting shot-point distance is about 17 m. Twenty-three seismic lines of northeast–southwest- and southeast–northwest-orientation in 3–5 km spacing were acquired (Fig. 2) and processed. Additional details on acquisition techniques are given in the P-336 cruise report (Kopf et al., 2006). We use Vista software (Seismic Image Software Ltd.) for standard processing of data, including trace editing, Common-Mid-Point (CMP) sorting, static and delay corrections, normal moveout corrections, bandpass frequency filtering (frequency content: 55/110–600/800 kHz), stacking, and migration (1500 m s^{-1}). A CMP spacing of 10 m is applied throughout. The Kingdom Suite (Seismic Micro-Technology Inc.) was used for seismic data visualization and interpretation.

3.3. Morphometric analysis

According to morphometric analysis of slope failure *sensu* McAdoo et al. (2000), we use the newly acquired seismic and bathymetry data to measure gradient values of the undisturbed slope adjacent to landslide scars, heights and slopes of headwalls, areas of seafloor affected by failure, failure depths, and estimate eroded sediment volumes as well as the runout distance of slides where identifiable. The morphometric analyses comprise comparisons of the measured features to a compilation of 'cohesive' vs. 'disintegrative' slope-type failures presented in McAdoo et al. (2000).

4. Observations from acoustic data

4.1. Relief and seafloor morphology from bathymetric data

In the study area northeast off the Bay of Mirabello, the Cretan shelf drops down towards the increasingly inclined slope (1–8°) and the steep southwestern flank of the Kamilonisi Basin (≥8°; Figs. 1B and 2A). The southwestern part of the investigated slope area shows a smooth seafloor morphology and topography of the upper slope region (≤3°; Fig. 2A). Towards the northeast further down the slope, the relief of the slope is more irregular and composed of small, northeast–southwest-trending topographic highs and lows (Fig. 2A). Below the mid-slope region, which is of 3–5° mean inclination, the seafloor drops off to the lower slope and the southwestern flank of the Kamilonisi Basin (Fig. 2A). The central part of the investigated area is

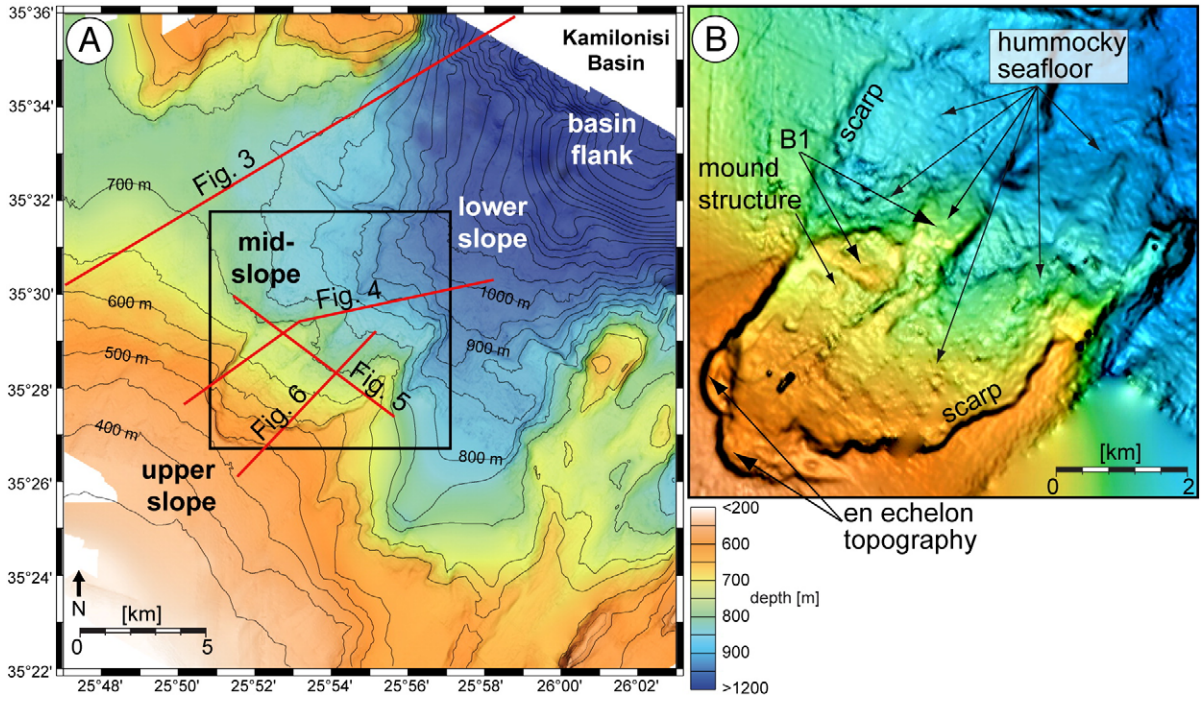

Fig. 2. A: The newly recovered bathymetric chart (shaded relief + colour) of the investigated area. Thin lines represent relief counter lines in 50-m intervals. Red lines indicate locations of seismic profiles shown in subsequent figures; B: close-up of the scar-structure in the central study site, showing steep outer walls, a hummocky seafloor morphology within the structure and an en echelon topography along the southwestern-most boundary. Note the block ('B1') of smooth morphology within the scar.

dominated by a downslope-concave scarp heading northeast (Fig. 2B). The seafloor morphology within the scarp as well as in an area further downslope is irregular and hummocky (Fig. 2B). In closer inspection, a narrow area of 'en echelon' topography is identified along the head region of the scarp (Fig. 2B). Additionally, a large block associated to the intact slope apron can be traced from the western boundary to the central part of the scarp (Fig. 2B).

4.2. Seismic characterization of sediments

In this study, we define seismic units in terms of deposits from gravitational mass-transport in contrast to undisturbed strata using seismic reflection pattern attributes, such as amplitude, continuity and configuration. As reasoned below, we identify three types of features: (1) the background unit U1 (Figs. 3–6), (2) scars as source areas of MTDs (SC1–3; Figs. 4–6), and (3) deposits from gravitational mass movement (MTD1–3; Figs. 4–6).

4.2.1. Background sediments (U1, B1, drape)

The background unit U1 is characterized by a parallel- to sub-parallel-, well-stratified reflector pattern showing occasionally small-scale reflector offsets. It represents regularly accumulated sediment on top of a gently inclined acoustic basement and post-depositional faulting (Figs. 3–6), which most likely represents the Messinian–Pleistocene boundary (5.332 ± 0.005 Ma (Krijgsman et al., 1999; see also seismic data interpretation in Mascle and Martin, 1990). In shallower water depths (i.e. <800 m), the slope shows a mostly undisturbed, continuous U1 pattern, except for those places where the regular pattern has been affected by erosional scars (see Section 4.2.2). The steeper slope as well as the following Kamilonisi Basin flank in >800 m water depths are almost devoid of the U1 pattern (e.g., Fig. 3). Measured values of mean U1-reflector inclination and approximated U1 thicknesses above the acoustic basement are presented in Table 1.

4.2.1.1. Faults. Faults within U1 are generally identified from offsets of seismic reflectors and mostly occur as straight to listric lineaments of various scales. We interpret two major trends of faults in the investigated area. The first and dominant pattern can be traced in approximately northeast–southwest direction (Figs. 5 and 7), while the second pattern occurs almost perpendicular trending approximately slope-parallel southeast–northwest (e.g. Figs. 3, 4 and 7).

Larger normal faults with partially high offsets in the southeastern extremity of the study area (Fig. 5) follow the overall northeast–southwest-trending main fault system of the southeastern Cretan Sea

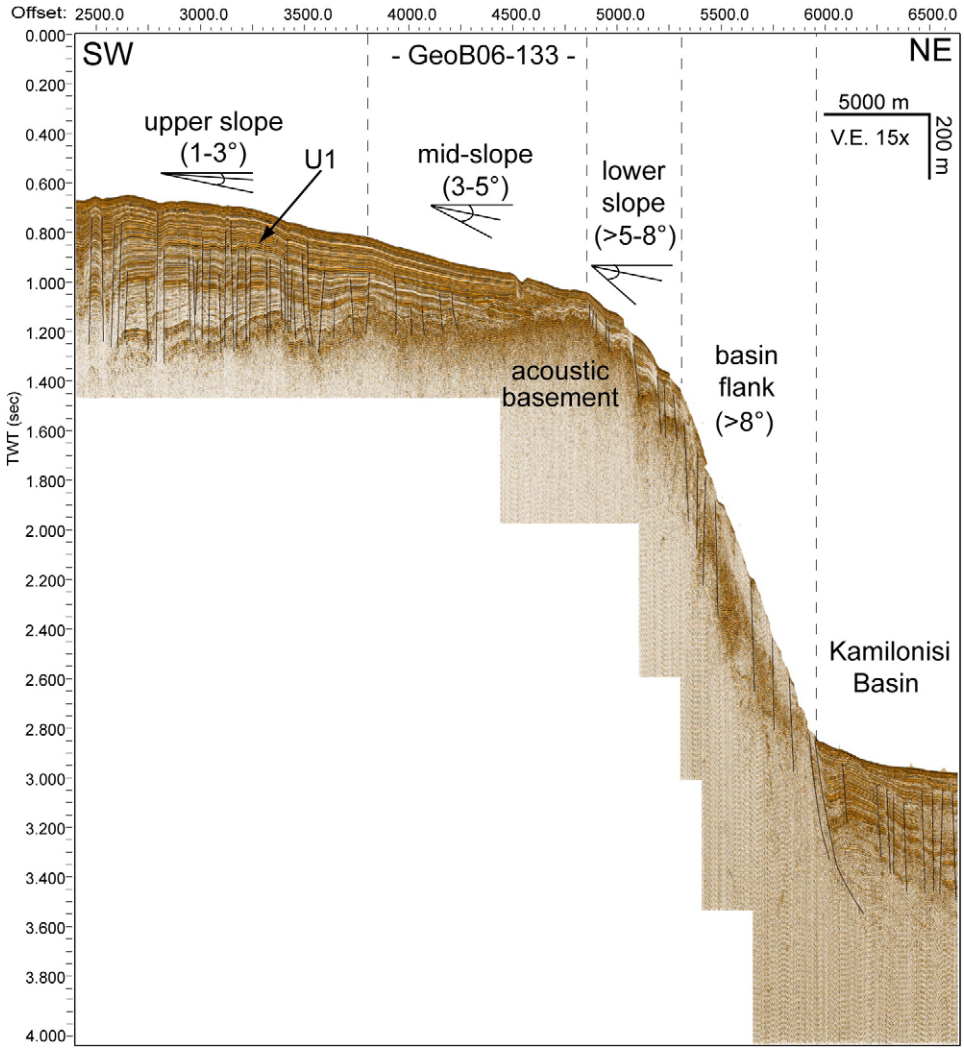

Fig. 3. Southwest–northeast seismic profile GeoB06-133 (for location see Figs. 1 and 2), showing the approximated positions of the upper, middle, and lower slope, transposed from the study site to this profile, as well as the Kamilonisi Basin flank and the foot region of the slope (Fig. 2). Note that the well-stratified U1 background sediment can be traced throughout the upper and mid-slope, while it is missing at the lower slope and the basin flank. Further note that slope angles as well as the slope part boundaries are projected from the closer study site (Fig. 2).

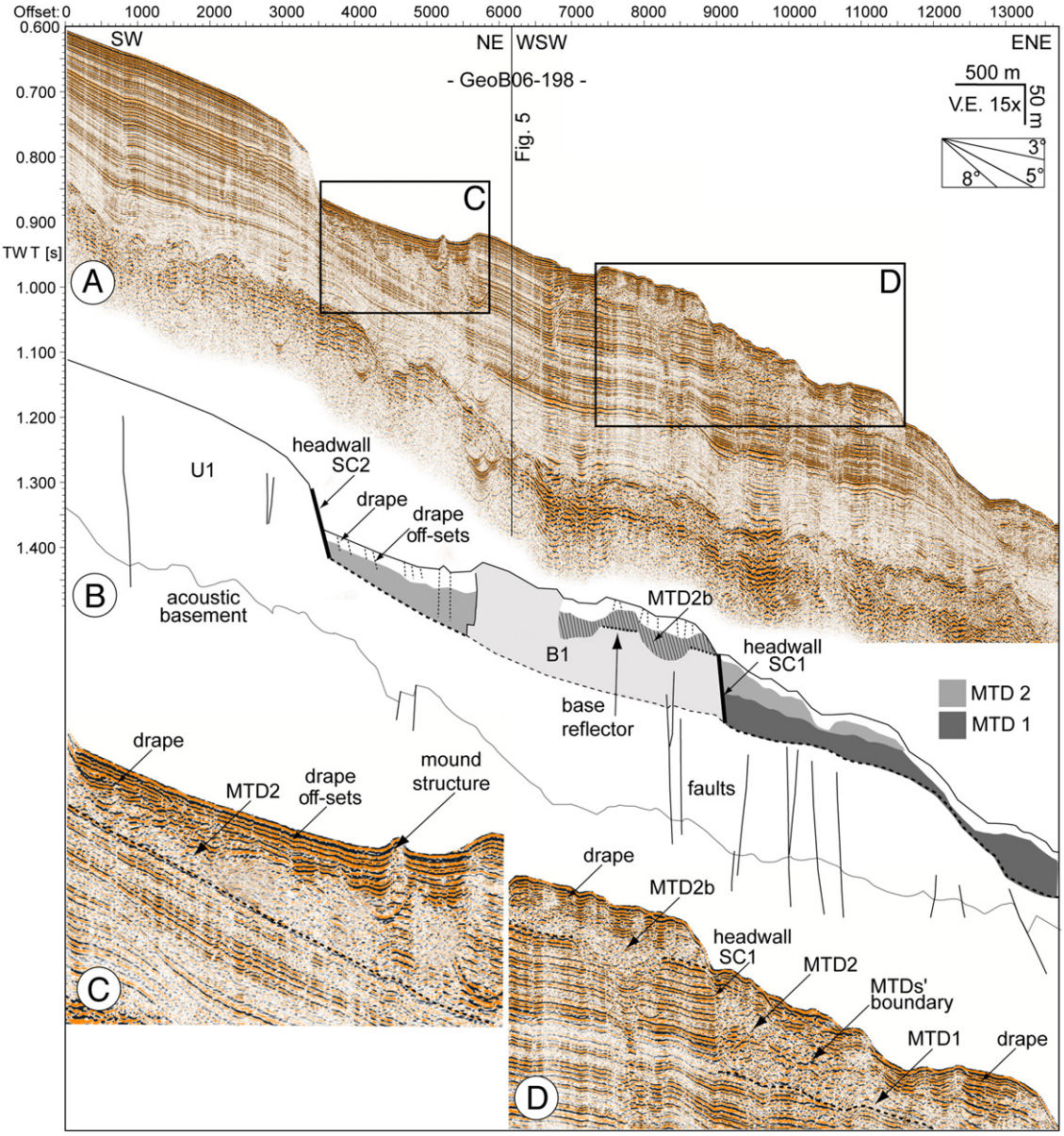

Fig. 4. A: Southwest–northeast seismic profile GeoB06-198 slicing the northern and central portion of the prominent scar, turning from a SW–NE-trend to a WSW–ENE-trend at the height of the 'B1'-block (for location see Fig. 2); B: sketch of the interpreted seismic unit MTD1 (dark grey), 2 (grey) and 2b (grey with lines), their scars SC1 and SC2 (headwalls thick, black lines), and the background units U1 (white) and 'B1' (light grey). Faults are marked as black lines, whereas small offsets in the drape on top of MTDs are marked as thin, dotted, black lines; C: close-up of the as MTD2 interpreted seismic unit in front of the interpreted headwall of SC2. Note that the MTD basis (dotted line) is almost parallel to the background sediment pattern below; D: close-up of the interpreted MTD2-sub-unit MTD2b on top of the 'B1' block (left) and the superposition of MTD2 on top of MTD1 in front of the SC1 headwall (right). The slope strata-parallel MTD bases are marked as thin dotted lines.

(see Section 2; Mascle and Martin, 1990). Most of these faults are related to steep relief structures identified in the bathymetric chart (e.g., Fig. 7), which is also in-line with a regional major fault-scarp interpretation by Angelier et al. (1982). Hence, these faults follow main structural elements of topographic highs and lows and can be correlated to the Cretan Sea basin extension and associated half graben formation (Mascle and Martin, 1990).

The second, almost perpendicular fault pattern comprises smaller and more scattered faults that often assemble in areas of pronounced changes in slope inclination, e.g. the slope breaks from the lower to the mid-slope and from the mid-slope to the upper slope (e.g., Figs. 3 and 4). They further concentrate on the shallower upper slope where they prepare a dense pattern of subordinated horst and graben structures, while they are almost missing in some parts of the mid-slope (Fig. 3). Towards the steeper lower slope and the Kamilonisi Basin flank, faults of this pattern again increase in number, size and are of high offset (Fig. 3).

4.2.1.2. Stable block 'B1'. A 2-km²-sized block of intact U1-stratification that occurs at the northwestern sidewall of SC2 (see Section 4.2.2) is referred to as 'B1' (e.g. Figs. 4 and 5). As we are able to extrapolate the B1 reflection pattern continuously to U1 upslope SC2, this structure is interpreted to represent a stable block of unmoved U1-succsession within SC2 as well as MTD2 (see Section 4.2.3; Fig. 7). Furthermore, the northeastern part of this block is partially covered by a MTD (MTD2b; See Section 4.2.3; Figs. 4B and 7). Geometrical proportions of B1 are presented in Table 1.

4.2.1.3. Drape. Also as part of U1, a uniform post-failure drape is interpreted on scars and on top of MTDs (Figs. 4–6). Measured drape thicknesses range between 10 and 20 m ($\pm$2.5 m), while drape thicknesses less than 5 m expected along steeper, exposed relief parts are barely identifiable according to the resolution of seismic data (i.e., 5 $\pm$ 2.5 m). In contrast to well- and parallel- to sub-parallel-stratified

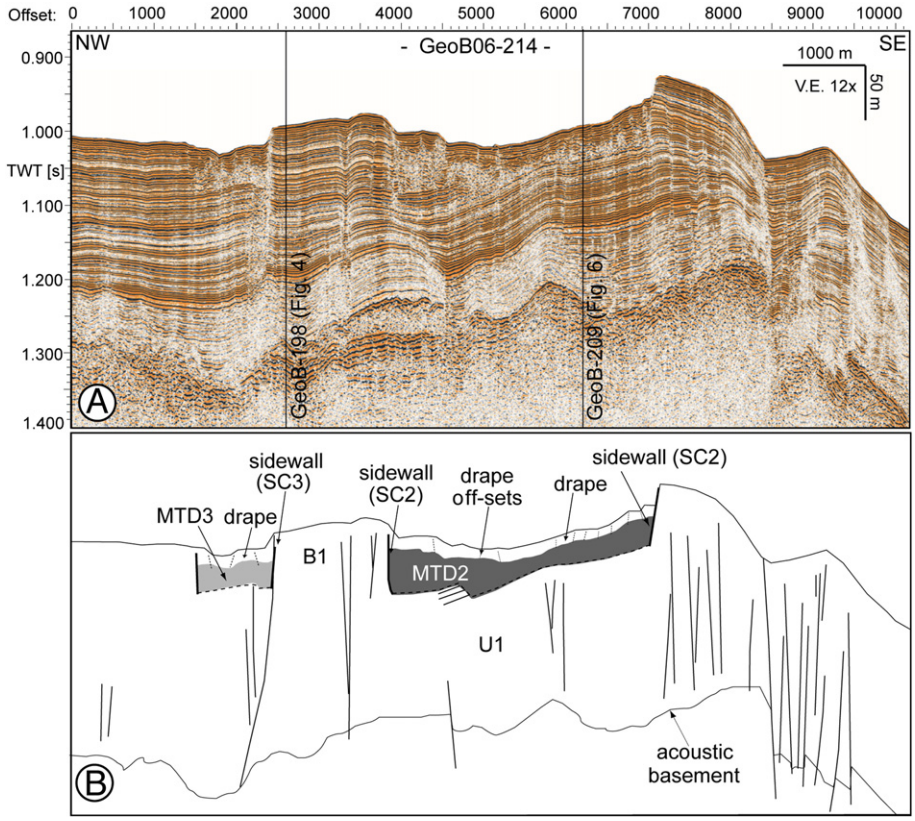

Fig. 5. A: Northwest–southeast seismic profile GeoB06-214 (for location see Fig. **2**), slicing the prominent scar (Fig. **2**B) slope-parallel and perpendicular to the transport direction of mass movements; B: interpretation figure of MTD2 (grey), sidewalls of SC2, the stable block B1 and MTD3 (light grey) as well as sidewalls of SC3. Black lines indicate interpreted faults, dotted line below MTDs the interpreted almost U1 pattern-parallel MTD basis.

draping sediments, those on top of (at least) MTD2 show a blocky, slightly rotational segmentation with some low-angle reflector offsets (Figs. 4–6). As these offsets are not correlatable to the general fault pattern described above (see Fig. 4A), they are inferred to originate from a deformation of the MTD after its deposition. Furthermore, we identify several vertically arranged anomalies in seismic attribute, which occur as lower reflection amplitudes within the MTD's drape (e.g. Fig. 4A and C). Below, within the MTD, they occur as higher

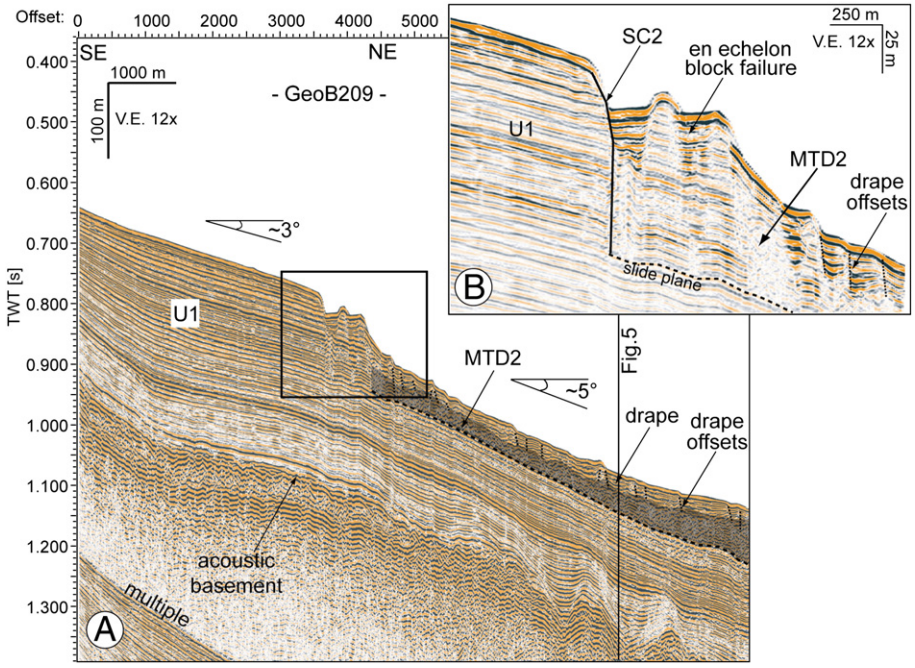

Fig. 6. A: Southwest–northeast seismic profile GeoB06-209 (for location see Fig. 2), slicing MTD2 (grey) in transport direction and the background unit U1. The black box represents a close-up of the headwall area shown in Fig. 6B; B: close-up on the headwall area of SC2 indicating failure of intact blocks along the wall that build up en echelon topography, and the MTD2 in front with typical, small offsets in the drape above.

Table 1
Geometrical measurements of scars (SC1–3), MTDs (MTD1–3) and background units (U1, B1).

	Surface (km²)	Thickness (m)	Gradient (°)	Volume (km³)	Water depths (m)
SC1	15	60[a]	25	0.9	900+
SC2	40	70[a]	16–23	2.8	500–800
SC3	6	40[a]	20	0.24	730–800
MTD1	20	40	5	0.8	>920
MTD2	50	50	5	2.5	520–1000
MTD2b	3	30	3	0.1	750–780
MTD3	12	25–30	4–5	0.36	750–900
U1	–	<100–>250	<1.4–5	–	<200–950
B1	2	75[b]	2–3	–	~720

[a] Maximum height of headwall.
[b] Thickness between MTD base reflector and seafloor.

reflection amplitudes compared to the MTD (e.g., Fig. 4C). Some of these seismic features further reach the topmost drape reflectors, rise above the seafloor and correlate to mound structures (e.g. Fig. 4C).

4.2.2. Scars

We define scars as volumetric features in-between head- and sidewalls down to slide planes, which equal volumes of eroded sediments. Head- and sidewalls are deep truncations of U1, indicating its erosion, with strong slope gradient increases up to 15–25° (Figs. 4–6). Scars are interpreted to originate from displacement of eroded U1-sediment and are correlated to mass wasting (Fig. 7). Further, we observe that orientation of side- and headwalls are of similar trend as interpreted faults, with headwalls and sidewalls tracing slope-parallel and the major northeast–southwest-trending fault system, respectively (Figs. 4, 5, and 7). Geometrical measurements of all scars are presented in Table 1.

"SC1" (Figs. 4 and 7) is the northeastern-most landslide scar detected in our data with a large and steep headwall (Figs. 4). Limited seismic data in this area do not indicate the presence of pronounced sidewalls. Although we don't have full control on scar's geometry and total extension due to less seismic data in this area, we can measure its headwall height and gradient as well as the gradient of the interpreted slide plane in front (Table 1).

A second scar "SC2" (Figs. 4–7) is present approximately 5 km upslope southwest of SC1 and imaged as a prominent mass-wasting structure in seismics as well as in bathymetry (see Section 4.1). SC2 consists of pronounced head- and sidewalls (e.g. Figs. 4 and 5), whereas the spacing between sidewalls is limited by the B1 block and therefore decreases with increasing water depth (Fig. 7). The headwall area further shows several wall-parallel blocks of almost intact U1-stratification with small vertical and lateral offsets (Fig. 6A and B). The blocks' displacement results in the prominent en echelon topography identified in bathymetric data (compare Figs. 2 and 7; see also Section 4.1).

The third detected landslide scar "SC3" is located at the northwestern boundary of SC2 (Fig. 7; see sidewalls in Fig. 5) and is of similar geometry and orientation as SC2, but much smaller in lateral extent and depth (Fig. 5; see also Table 1). Note that the northwestern sidewall of SC3 occurs as an extension of the northern sidewall of SC2 (see Fig. 7), while its head- and southeastern sidewall trace the steep flanks of the B1 block (Fig. 5; see also Section 4.2.1.2).

4.2.3. MTDs

Three MTDs are identified as confined bodies of chaotic to nearly transparent reflection patterns, indicating different grades of deformation of eroded U1 sediment during transport, thus strongly contrasting intact U1 (e.g. Figs. 4 and 6). Measured geometrical proportions of all MTDs and gradients of slide plane reflectors below are comprised in Table 1.

MTD1 occurs frontal northeast and downslope of SC1 in seismic data (Figs. 4 and 6). As SC2 and SC3 cannot explain the volume of this MTD, as well as it is overlain by MTD2, we interpreted SC1 being its source scar (Fig. 7). MTD1 is of varying thicknesses, resulting in an irregular contact with the overlying, draping U1-sediments (Fig. 4A and B). Note that the basis of this MTD can be traced parallel to the intact seismic reflection pattern below (dashed line in Fig. 4B).

MTD2 (Figs. 4–7) is mostly present within SC2 in front of the headwall (Figs. 4B and 6) and between sidewalls (Fig. 6), which is thus identified as its source scar. The basis of the downslope increasingly chaotic pattern of MTD2 is almost parallel to the intact seismic reflection pattern below, which further appears to correlate to the stratigraphically depth of the base of MTD1 (Fig. 4B). Further, seismic data reveal that a portion of MTD2 covers MTD1 in front of SC1 (Figs. 4B and 7). The boundary between both MTDs is indicated by some less-deformed reflectors patches at the top of MTD1 contrasting the nearly transparent reflection pattern at the bottom side of MTD2 (Fig. 4B). Since these less-deformed reflector patches do not occur further downslope northeast in our data, we interpret them representing less-deformed slid sediment at the top of MTD1.

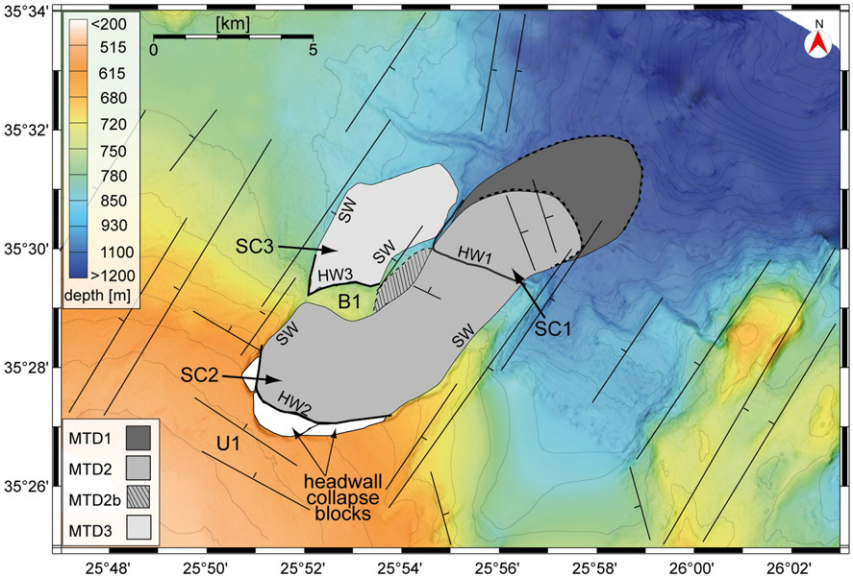

Fig. 7. Bathymetry map-plot of the investigated area with interpreted (dashed lines = assumed) lateral extents of MTD 1, 2, 2b, 3, SC1, 2, 3, and B1. All non-marked areas primarily belong to the background unit U1. Interpreted main faults are marked as black lines and dips; SW: sidewall; HW: headwall.

Another portion of MTD2 is referred to as the sub-unit MTD2b, identified as a relatively thin, chaotic, and irregular slide deposit on top of the northeastern extension of B1 (Fig. 4B; see also Section 4.2.1). The assumed linkage of this slide deposit to the development of MTD2 is based on the stratigraphic depth of the MTD2b basis which correlates with the stratigraphic depth of the assumed seafloor at the time of MTD2 emplacement (i.e. recent seafloor minus MTD drape thickness; Fig. 4A and B). Hence, both MTDs are suggested being of about same age and can be genetically linked.

MTD3 is, compared to MTD1 and MTD2, a small landslide deposit (see Table 1) and located almost completely within its source scar SC3 (Figs. 5 and 7). This MTD's slide plane also occurs almost parallel to the seismic reflection pattern below, but found in stratigraphically shallower depth compared to those of MTD1 and MTD2 (Fig. 5).

5. Interpretations

5.1. Timing and evolution of slope failure and mass movements

Based on our observation of sizes, locations and a sequencing of MTDs as well as sizes and locations of their source scars, we here compile a conceptual model of slope-failure development. We focus on mass-movement transport paths and runout distances as well as the relative arrangement of MTDs to reconstruct a relative timing of single failure events. As a basis for our model, we use a pre-failure slope geometry (Fig. 8A) reconstructed from (i) a transposed, intact seismic reflector from depth (e.g., Fig. 4B), (ii) measurements of intact slope geometry from bathymetric and seismic data adjacent to the failed slope (e.g., Figs. 2 and 3), and (iii) the intact portion of the interpreted deposition reflector of MTD2b (Fig. 4B).

5.1.1. Initial failure phase

Our reconstruction of an initial phase of slope destabilization is at least based upon the stratigraphic arrangement of MTD2 on top of MTD1 (see Section 4.2.3) indicating that MTD1 emplaced prior to MTD2. We assume that an external trigger mechanism, e.g. an earthquake (as proposed by Chronis et al., 2000 and Kopf et al., 2006, 2007) is responsible for initializing sediment destabilization at the steeper mid-slope (i.e. 5°) along the headwall of SC1 (Fig. 8A and B). Consequently, downslope movement of an up to 60-m-thick sediment package along an inclined slide plane towards the northeast occurred (Fig. 8B). According to increase in slope angle (≥8°) further northeast downslope, we infer that a portion of this landslide could have been transported further down the steeper slope out of data range, whereas a large MTD portion accumulated in front of the headwall. This depletion of sediment along SC1 is suggested to have acted as a pre-conditioning factor for destabilization of further sediments upslope.

5.1.2. Retreating failure phase

We reconstruct this second phase of slope destabilization in terms of sediment failure retreating upslope towards the southwest. We interpret that sediments were destabilized in the back of SC1, have overridden the headwall, and accumulated as portion of MTD2 on top of MTD1 (Fig. 8C).

As we see here some analogies in scar and MTD geometry to well-documented studies on retreating landslide complexes (see data in e.g. Kvalstad et al., 2004 and L'Heureux et al., 2007), we are tempted to combine the described MTDs and their scars to a landslide complex.

It is difficult to assess whether all masses of MTD2 failed simultaneously or with intervening time-periods. However, as we are not able to identify individual slide bodies within MTD2 in seismic data, this MTD may originate either from a single or several phases of sediment destabilization in a short time-period upslope towards the southwest. With respect to the resolution of our seismic data (i.e., 5±2.5 m), we admit maximum possible intervening periods in the order of 25–70 ka based on sediment accumulation rates of between 7 and 20 cm ka^{-1} for this region of the slope (e.g., Chronis et al., 2000; Giresse et al., 2003; Strozyk et al., 2009).

In closer inspection of the retreating failure development, the presence of the stable B1-block in the area of SC2 suggests that the

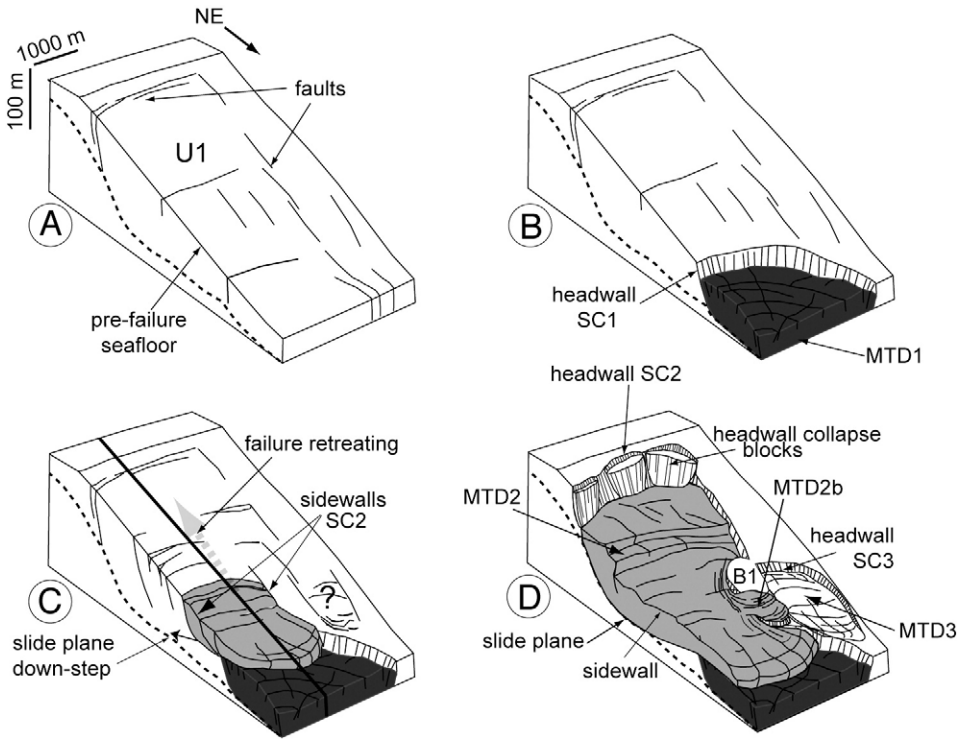

Fig. 8. Time series of 3D-sketches showing the landslide complex evolution: A: reconstructed pre-failure setup; B: initial failure along SC1 and deposition of MTD1; C: failure retreating upslope towards the southwest, maybe also failure of masses within SC3; D: emplacement of MTD2 and possibly MTD3; uncoupling of failure along minor slope-parallel faults resulting in the headwall of SC2.

northeastern landslide portion was destabilized in upslope direction forming the narrowing passage in-between B1 and the southeastern sidewall of SC1 (Fig. 8C–D). Here, the slide plane of the MTD2-landslide is present at the same stratigraphic level as the top of the previously accumulated MTD1 (see Fig. 8C). We further interpret that the depth of failure stepped down to the pronounced, intact U1 reflection-parallel MTD basis during the failure retreating somewhat further upslope in the back of SC1 (Fig. 8C to D). This may imply the presence of a mechanically weak(er) sediment layer in depth, which may be responsible for this preferred depth of sediment failure (i.e. MTD1 and MTD2) as well as plane-parallel sliding of masses on top. Alternatively, the stability conditions of this slope may have been critical at this stratigraphic level, at which an interplay between the relative increase in overburden stress with increasing depth and the increase in strength with increasing depth due to sediment consolidation may result in a critical stratigraphic window of low(er) stability (particularly when agitated by transient stresses during e.g. earthquake shaking; Lee et al., 2007). However, coevally the destabilized sediments spilled across some remaining, intact U1-strata in the back of SC1, then have overridden the headwall of SC1 and finally accumulated on top of MTD1 (Fig. 8D).

Another portion of slid masses associated to the development of MTD2 is reconstructed to have been transported along the northwestern sidewall of SC2 and to have overridden the southeastern flank of B1 (Fig. 8D). While B1 remained stable during the complex evolution, this small slide portion (MTD2b) accumulated on the top of the block's northeastern extension (Fig. 8D).

As a result from this slope-failure development, the larger volume of the MTD2-landslide is found in front of the head- and in-between the sidewalls of its source scar. However, it is likely that a northeastern-most portion also of this landslide experienced longer runout downslope out of data range.

In a final stage of the evolution of the landslide complex, coherent, triangular blocks of almost intact U1-stratification failed along the SC2-headwall and built-up the en echelon topography described from both seismic and bathymetry data (Figs. 2B, 6B, and 8D). We suggest that the most proximal part of the recently accumulated MTD2 restricted further downslope movements of these blocks. This 'headwall collapse' traces the slope break that separates the mid-slope (5°) and upper slope region (3°). Hence, we deduce that this sagging of blocks at this particular slope break position finally uncoupled sediment failure upslope towards the southwest (Fig. 8D).

5.1.3. MTD3

The failure of masses deposited as MTD3 cannot be arranged in stratigraphic order to the other MTDs. As this landslide shows a very short runout, no sequenced bedding and thus no chronology relative to other MTDs can be determined. However, the drape thickness on top of MTD3 is almost identical to that of the entire complex, thus indicating a roughly similar age and allowing us to propose this event to have occurred coevally to the development of this landslide complex (Fig. 8C–D).

5.1.4. Post-slide phase

Since the emplacement of the MTDs, constant draping of sediments to the currently detectable 10–20-m-thick background sediment on top of MTDs occurred. Short distant creeping is deduced for at least MTD2-overlying strata as indicated from a slightly rotational deformation of drape on top of the MTD in downslope direction (Figs. 4 and 6). This deformation is interpreted to coincide with a de-watering of MTD2 to the drape, resulting also in some fluid-escapes at the seafloor. The acoustically-transparent, vertically arranged anomalies in seismic amplitude observed in e.g. seismic profile GeoB-198 (Fig. 4A and C) likely support this interpretation of fluid-escape features, as similar structures have been related to such processes in other settings (e.g., Moernaut et al., 2009). These processes likely indicate that MTD2-overlying strata as well as maybe also the MTD have not been consistently of steady state since landslide deposition and the subsequent background sediment accumulation. Furthermore, this may also indicate an ongoing tectonic movement and steepening of at least this Cretan slope portion after MTD deposition.

5.2. Identification of mass-movement types

Our interpretation of failure and transport mechanisms of mass movement at the study site is based on the general landslide nomenclature by Hampton et al. (1996) and Lee et al. (2007). Interpreted source scars (SC1–3) and slide planes as well as MTD geometries, internal deformation patterns, transport paths, and runout distances are considered for their classification.

All landslides and MTDs detected and investigated at the study site have been released and moved or have accumulated, respectively, along more or less distinct slide planes as indicated by MTD bases parallel to the intact background sediment pattern below. We interpret translational sliding along those surfaces to be the dominant transport mechanism. The degree of internal deformation of MTDs implies relatively high transport dynamics and thus slow movement is unlikely despite short runout distances. This is in line with a rough comparison of scar and MTD volumes implying that the larger portions of MTDs are most likely found within or close to source scars.

Nevertheless, the volumetric comparisons as well as the downslope increasing slope gradient (>5°) may also imply that not the entire eroded masses deposited after short runout at the mid-slope. We suggest movement of masses also down towards the steeper lower slope northeast. Strozyk et al. (2009) found evidence of both landslide and mass-flow deposits in a nearby area of the northeastern Crete slope and propose that larger runouts of slides can cause their disintegration to mass flows. Based on that, we propose that a similar behaviour may also apply to former landslides as well as missing portions of here described landslides generated in this slope region if their transport down to the steeper lower slope has lead to an increase in transport dynamics. This most likely caused disintegration of these primary cohesive landslides and enabled their further movement as debris or mass flows all the way down to the slope foot region. This interpretation is in line with seismic data showing multiple stacked MTDs in the Kamilonisi Basin (Kopf et al., 2006).

6. Discussion and conclusions

We have shown that the multiple MTDs found in a mid-slope position on the northeastern Cretan margin originate from deposition of coherent sediment masses after short distant sliding along well-defined slide planes close to their source scars. Thereof, a first event was possibly triggered by an external stimulus (e.g., earthquake) and its depletion acted as a pre-conditioning factor for a destabilization of additional sediment packages further upslope. We observe that neither stable background sediments, nor MTDs can be found on the steeply inclined lower slope and Kamilonisi Basin flank further downslope this first MTD. Opposite, background sediments of the shallower, lower inclined slope are still intact and stable (e.g., Figs. 2–4; see also Kopf et al., 2006, 2007). A structural interpretation of two main fault patterns within the background sediment in the vicinity of the landslide scars implies that the sum of fault offsets in downslope direction may be higher within this critical mid-slope portion and scar areas compared to the stable slope apron. This would be in line with our gradient measurements of MTD bases, which thus show higher values of at least 5° within the scars (Table 1). Hence, fault activity is likely responsible for the higher slide plane inclination, which is thus inferred to be a critical threshold and pre-conditioning factor for sediment destabilization as well as it allows deposition of coherent landslides in the mid-slope.

In terms of mass wasting producing landslides at the size of the detected MTDs, the investigated slope area can consequently be

subdivided into (1) a currently stable upper slope (1–3°), (2) a partially critical inclined mid-slope (3–5°), and (3) an over-critical lower slope (>5°; Figs. 3 and 9). Initiation of landsliding at the critical mid-slope as well as uncoupling of failure at the break from the mid-slope to the upper slope may further indicate a restriction of youngest slope collapses to well-defined, critically-inclined slope regions. We therefore deduce that slope geometry of pronounced breaks in slope angle may be an important pre-conditioning factor for (repeated) sediment destabilization besides external trigger mechanisms (see Fig. 9).

On closer inspection, our measurements of source scars show some morphometric analogies to 'cohesive failures' described in the literature (McAdoo et al., 2000). These analogies include small failure areas (12–50 km²), while headwalls are steep (15–25°) and the failure depths are high (~60 m). Also the landslide deposits show similarities to the morphometric characteristics of 'cohesive slides' (McAdoo et al., 2000) as they are of short runout (<1–5 km) compared to the heights of their headwalls, and deposited as compact, coherent MTDs (≤2 km³). This at first high coherency of destabilized masses is held responsible for their short runout and deposition of MTDs close to scars, thus characterizing this portion of the northeastern Cretan slope as a 'cohesive slope'.

On the other hand, important differences to settings characterized as 'cohesive slopes', e.g. forearc slopes at accretionary margins (McAdoo et al., 2000), are attributed to the Cretan margin tectono-sedimentary setting that is dominated by hemipelagic sedimentation on an extensional basin slope. Thus, the slope-parallel sediment bedding is held responsible to favour translational mass movement along well-defined slide planes of 5° inclination, which is below typical values for 'cohesive slope failure'-examples that often occur as deeply incised slumps (McAdoo et al., 2000). McAdoo et al. (2000) further propose that typical 'cohesive failures' tend to make a slope steeper whereas the mass wasting observed at the northern Cretan margin indicates that the taper can also be adjusted by translational mass movements. Also, if landslides reach the steeper, lower slope that appears to exceed a threshold gradient for deposition, runout distances can be large and cause a disintegration of the coherent landslides into mass flows.

In conclusion, our study suggests that northeast Cretan slope mass-wasting events at the scale of observed scars and MTDs typically occur in narrow, well-defined and critically steepened slope portions. The youngest events can thus be found in a mid-slope position (Fig. 9). On longer time-scales, an upslope relocation of this critical area to its current position may have occurred. This relocation was most likely controlled by the progressive steepening of this slope, caused by the uplift of Crete and the counter movement from Kamilonisi Basin subsidence (e.g., Stavrakakis et al., 2000; Fig. 9). We suggest that source areas of deeply-buried, older MTDs in the Kamilonisi Basin occurred at lower slope portions. High subsidence rates in the basin then caused an over-critical inclination of the lower slope and basin flank, and the upward extension of the slope area critical for mass wasting over longer time-scales. This mechanism may have caused further transport of former landslides or a reactivation of their MTDs down to the slope foot region, as expressed in the multiple Kamilonisi Basin MTDs (Fig. 9). Consequently, evidence for mass wasting of larger scale in sediments of the investigated slope portion is only present in scattered, youngest mid-slope MTDs and their associated scars, tracing the narrow, critically inclined slope portions. This conceptual model may likely explain how such active margin settings can exhibit only scarce findings of MTDs on the slope while evidence for an extensive and widespread mass wasting is expected due to high neotectonic activity.

Acknowledgements

We thank the whole scientific party and the ship crew of P-336 for faithful and detailed recording of data. We thank all involved scientists at the Hellenic Centre for Marine Research, Greece, for their scientific input and discussions as well as support of the P-336 cruise. We thank the MARUM for scientific support and involved

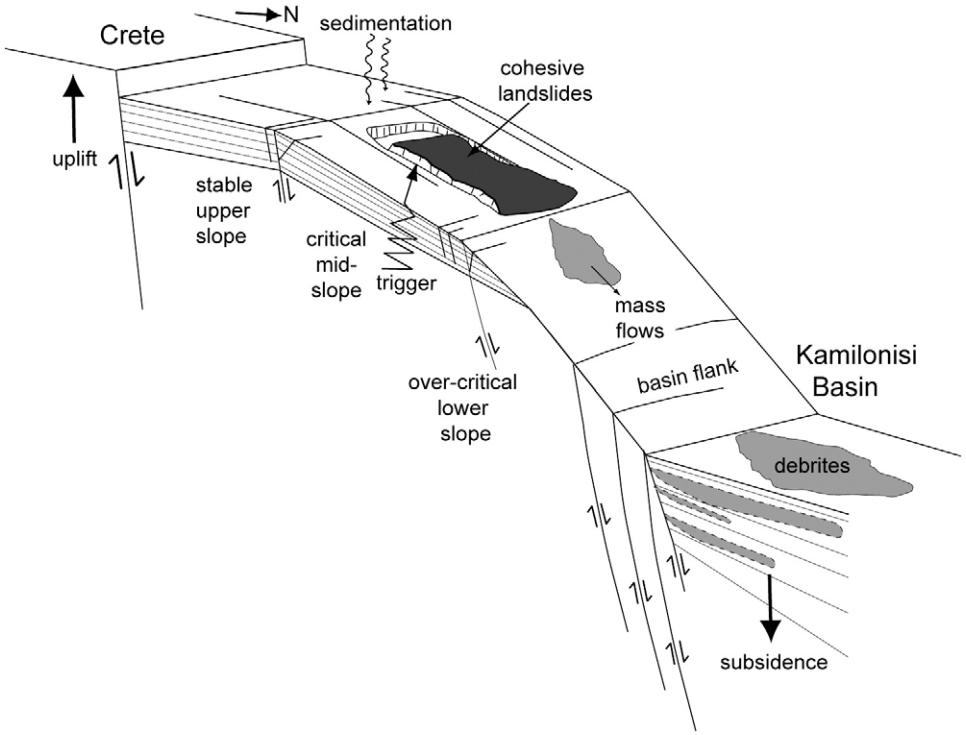

Fig. 9. Sketch of mass-movement development of the investigated northeastern Cretan slope (not to scale). Note that we infer that an external stimulus (e.g., earthquake trigger) is required to cause landsliding in the critical mid-slope region. The resulting landslides can either deposit in the critical mid-slope region or, if they reach the steeper lower slope, being transported further downslope immediately or after reactivation (i.e. in response to further steepening), disintegrate into mass flows, and finally deposit as debrites in the Kamilonisi Basin. Both the 'critical' and the 'over-critical' slope portions are suggested to have relocated in upslope direction through time in response to high basin subsidence as well as the countering uplift of the island of Crete. This entire mechanism may already have eroded and continue to erode the post-Messinian Cretan slope sediment load.

scientists for fruitful discussions. Further we would like to thank Marc De Batist and a second, unknown reviewer for their fruitful comments and suggestions that highly improved the quality of the paper. This publication is funded through the DFG-Research Centre/Cluster of Excellence “The Ocean in the Earth System”.

References

Angelier, J., Lyberis, N., Le Pichon, X., Barrier, E., Huchon, P., 1982. The tectonic development of the Hellenic arc and the sea of Crete: a synthesis. Tectonophysics 86, 159–196.

Bonneau, M., 1984. Correlation of the Hellenide nappes in the south-east Aegean and their tectonic reconstruction. Geological Society, London, Special Publications 17, 517–527.

Canals, M., Lastras, G., Urgeles, R., Casamor, J.L., Mienert, J., Cattaneo, A., De Batist, M., Haflidason, H., Imbo, Y., Laberg, J.S., Locat, J., Long, D., Longva, O., Masson, D.G., Sultan, N., Trincardi, F., Bryn, P., 2004. Slope failure dynamics and impacts from seafloor and shallow sub-seafloor geophysical data: case studies from the COSTA project. Marine Geology 213, 9–72.

Caress, D.W., Chayes, D.N., 1996. Improved processing of Hydrosweep DS multibeam data on the R/V Maurice Ewing. Marine Geophysical Resarch 18, 631–650.

Chronis, G., Lykousis, V., Anagnostus, C., Karageorgis, A., Stavrakakis, S., Poulus, S., 2000. Sedimentological processes in the southern margin of the Crete Sea (NE Mediterranean). Progress in Oceanography 46, 143–160.

Ganas, A., Parsons, T., 2009. Three-dimensional model of Hellenic Arc deformation and origin of the Cretan uplift. Journal of Geophysical Research 114, 1–14.

Gee, M.J.R., Masson, D.G., Watts, A.B., Allen, P.A., 1999. The Saharan debris flow: an insight into the mechanics of long runout submarine debris flows. Sedimentology 46, 317–335.

Giresse, P., Buscail, R., Charriere, B., 2003. Late Holocene multisource material input into the Aegean Sea: depositional and post-depositional processes. Oceanologica Acta 26, 657–672.

Haflidason, H., Sejrup, H.P., Berstad, I.M., Nygård, A., Richter, T., Bryn, P., Lien, R., Berg, K., 2003. A weak layer feature on the Northern Storegga Slide escarpment. In: Mienert, J., Weaver, P. (Eds.), European Margin Sediment Dynamic — Side-Scan Sonar and Seismic Images. Springer, Berlin, pp. 55–62.

Haflidason, H., Sejrup, H.P., Nygård, A., Mienert, J., Bryn, P., Lien, R., Forsberg, C.F., Berg, K., Masson, D., 2004. The Storegga Slide: architecture, geometry and slide development. Marine Geology 213, 201–234.

Hampton, M.A., Lee, H.J., Locat, J., 1996. Submarine landslides. Reviews of Geophysics 34, 33–59.

Kopf, A., Alves, T., Heesamnn, B., Irving, M., Kaul, N.E., Kock, I., Krastel, S., Reichelt, M., Schäfer, R., Stegmann, S., Strasser, M., Thölen, M., 2006. Report and preliminary results of Poseidon cruise P336: CRESTS — Cretan Sea Tectonics and Sedimentation, Heraklion 28.04.-17.05.2006. Berichte, Fachbereich Geowissenschaften, Universität Bremen, 253.

Kopf, A., Stegmann, S., Krastel, S., Förster, A., Strasser, M., Irving, M., 2007. Marine deep-water free-fall CPT measurements for landslide characterisation off Crete, Greece (Eastern Mediterranean Sea) — part 2: initial data from the western Cretan Sea. In: Lykousis, V., Sakellariou, D., Locat, J. (Eds.), Submarine mass movements and their consequences. : Advances in Natural and Technological Hazards Series. Springer, pp. 199–208.

Krijgsman, W., Hilgen, F.J., Raffi, I., Sierro, F.J., Wilson, D.S., 1999. Chronology, causes and progression of the Messinian salinity crisis. Nature 400, 652–655.

Kvalstad, T.J., Andresen, L., Forsberg, C.F., Berg, K., Bryn, P., Wangen, M., 2004. The Storegga Slide: evaluation of triggering sources and slide mechanics. Marine and Petroleum Geology 22, 245–256.

Lee, H.J., Locat, J., Desgagnes, P., Parsons, J.D., McAdoo, B.G., Orange, D.L., Puig, P., Wong, F.L., Dartnell, P., Boulanger, E., 2007. Submarine mass movements on continental margins. In: Nittrouer, C.A., Austin, J.A., Field, M.E., Kravitz, J.H., Syvitki, J.P.M., Wiberg, P.L. (Eds.), Continental Margin Sedimentation. Blackwell Publishing, UK, pp. 213–274.

Leeder, M., 1999. Sedimentology and Sedimentary Basins — From Turbulences to Tectonics. Blackwell Publishing, UK.

Le Pichon, X., Angelier, J., 1979. The Hellenic Arc and Trench system: a key to neotectonic evolution of the Eastern Mediterranean area. Tectonophysics 6, 1–42.

L'Heureux, J.-S., Longva, O., Hansen, L., Vingerhagen, G., 2007. The 1990 submarine slide outside the Nidelv River mouth, Trondheim, Norway. In: Lykousis, V., Sakellariou, D., Locat, J. (Eds.), Submarine Mass Movements and Their Consequences. : Advances in Natural and Technological Hazards Series. Springer, pp. 199–208.

Locat, J., Lee, H.J., 2002. Submarine landslides: advances and challenges. Canadian Geotechnical Journal 39, 193–212.

Lykousis, V., Anagnostou, C., Anastasakis, G., Pavlakis, P., Roussakis, G., Alexandri, M., 1995. Quartenary sedimentary history and neotectonic evolution of the eastern part of Central Aegean Sea. Marine Geology 186, 281–298.

Masson, D.G., Harbitz, C.B., Wynn, R.B., Pedersen, G., Løvholt, F., 2006. Submarine landslides: processes, triggers and hazard prediction. Philosophical Transaction of the Royal Society A 364, 2009–2039.

Mascle, J., Martin, L., 1990. Shallow structure and recent evolution of the Aegean Sea: a synthesis based on continuous reflection profiles. Marine Geology 94, 271–299.

McAdoo, B.G., Pratson, L.F., Orange, D.L., 2000. Submarine landslide geomorphology, US continental slope. Marine Geology 169, 103–136.

McAdoo, B.G., Capone, M.K., Minder, J., 2004. Seafloor geomorphology of convergent margins: implications for Cascadia seismic hazard. Tectonics 23.

McKenzie, P.D., 1978. Active tectonics of the Alpine–Himalayan belt: the Aegean Sea and surrounding regions. Geophysical Journal of the Royal Astronomical Society 55, 217–254.

Meier, T., Rische, M., Endrun, B., Vafidis, A., Harjes, H.-P., 2004. Seismicity of the Hellenic subduction zone in the area of western and central Crete observed by temporary local seismic networks. Tectonophysics 383, 149–169.

Meulenkamp, J.E., Wortel, M.J.R., van Wamel, W.A., Spakman, W., Hoogerduyn Strating, E., 1988. On the Hellenic subduction zone and the geodynamic evolution of Crete since the late Middle Miocene. Tectonophysics 146, 203–215.

Moernaut, J., De Batist, M., Heirman, K., Van Daele, M., Pino, M., Brümmer, R., Urrutia, R., 2009. Fluidization of buried mass-wasting deposits in lake sediments and its relevance for paleoseismology: results from a reflection seismic study of lakes Villarrica and Calafquén (South-Central Chile). Sedimentary Geology 213, 121–135.

Perissoratis, C., Papadopoulos, G., 1999. Sediment instability and slumping in the southern Aegean Sea and the case history of the 1956 tsunami. Marine Geology 161, 287–305.

Stavrakakis, C., Chronis, G., Tselepides, A., Heussner, S., Monaco, A., Abbasi, A., 2000. Downward fluxes of settling particles in the deep Cretan Sea (NE Mediterranean). Progress in Oceanography 46, 217–240.

Strozyk, F., Huhn, K., Strasser, M., Krastel, S., Kock, I., Kopf, A., 2009. New evidence for massive gravitational mass-transport deposits in the southern Cretan Sea, eastern Mediterranean. Marine Geology 263, 97–107.

Urgeles, R., Leynaud, D., Lastras, G., Canals, M., Mienert, J., 2006. Back-analysis and failure mechanisms of a large submarine slide on the Ebro slope, NW Mediterranean. Marine Geology 226, 185–206.

Wessel, P., Smith, W.H.F., 1998. New, improved version of the generic mapping tools released. EOS Trans AGU 79, 579.